Molecular Crystals and Liquid Crystals
Publication details, including instructions for authors and subscription information:
http://www.tandfonline.com/loi/gmcl16

Small-and Wide Angle X-ray Scattering of Oriented Lecithin Multilayers

M. Hentschel [a] & R. Hosemann [a]
[a] Gruppe Parakristallforschung, c/o BAM, Kamillenstr, 21, D 1000, Berlin, 45, Germany
Version of record first published: 21 Mar 2007.

To cite this article: M. Hentschel & R. Hosemann (1983): Small-and Wide Angle X-ray Scattering of Oriented Lecithin Multilayers, Molecular Crystals and Liquid Crystals, 94:3, 291-316

To link to this article: http://dx.doi.org/10.1080/15421408308084264

Mol. Cryst. Liq. Cryst., 1983, Vol. 94, pp. 291–316
0026-8941/83/9403–0291$18.50/0

Printed in the United States of America

Small- and Wide Angle X-ray Scattering of Oriented Lecithin Multilayers†

M. HENTSCHEL and R. HOSEMANN

Gruppe Parakristallforschung, c/o BAM, Kamillenstr, 21, D 1000 Berlin 45, Germany

(Received September 21, 1981; in final form July 22, 1982)

It is the aim of this paper to demonstrate that much information is to be obtained about lamellar systems when diffraction work is performed on well aligned samples and paracrystal methods are applied. There is no need to examine "crystallized" monohydrates in order to get more diffraction spots. Contrary to this, a water content above 20% is of higher biological relevance. The water content of 23 wt.% was introduced by swelling in the gel-phase, giving a bigger stacking period than usually reported, when swelling is performed in the L_α-phase. At various temperatures oriented "multi-sandwiches" of dipalmitoyl lecithin (DPL) multilayers were analyzed by small- and wide angle X-ray diffraction as partly reported before. Thus, in the gel-phase the tilt angle φ of the hydrocarbon chains can directly be measured, and moreover it is proved that the chains are tilted by 7° to 15° in b-direction of the orthorhombic and the hexagonal lattice. 012-paraffine netplanes stabilize a well-defined membrane surface like the 201-planes in Cerebrosides. Contrary to paraffins the $c/2$ steps of the CH_2-chains along the b-direction are only a statistical average. These steps roughen the lamellae surfaces and produce paracrystalline distortions of $g \sim 2.4\%$ of the long period in the gel-phase. In the $P_{\beta'}$-phase φ diminishes monotonously because the number of $c/2$-shifts decreases. φ is zero in the L_α-phase and the CH_2-chains are laterally paracrystalline distorted with $g \sim 10\%$ and the membrane surfaces become smooth because molecular dynamics hinder the chains from latching on to each other, and the long period, therefore, is crystalline-like. Astbury's remarks on the interplay of order-disorder between molecular and supermolecular structures is fulfilled in a special way. In addition, the α^*-law, which combines the size of the lamellae bundles with their g-values also is fully confirmed.

Below 35°C the hydrocarbon lattice is orthorhombic with a 1% deviation from the hexagonal case. Only near 0°C undergoing the "subtransition" is the lattice similar to paraffins, and the tilt angle is reduced. The $P_{\beta'}$-phase is characterized by a hexagonal hydrocarbon lattice accompanied by the wellknown "ripples" which take the direction of the a-axis, making them orthogonal to the molecular tilt direction. Contrary to the findings of others our "weak" ripples produce no equatorial reflection in the small angle region, explained by the lack of longitudinal density fluctuations. A profound theoretical calculation of the weights of the humps at the long period tails yields ripple waves with a mean wave length of 310 ±30 Å and an

†Presented at "Ninth International Conference on Liquid Crystals", Dec. 6–10, 1982, Bangalore, India.

amplitude (4.5 ±0.5)Å. The wave lengths here vary to such a large amount that the small angle pattern offers no distinct isolated lateral spots. This is explained by the multi-sandwich preparation which hinders their free development. The analysis, with help of uncorrelated step dislocations, leads to a paracrystalline value of $g_{exp} = 10\%$.

I. INTRODUCTION

First X-ray studies of oriented DPL-multilayers by Levine[1,2] gave evidence of the hydrocarbon chains being tilted with respect to the layer normal in the gel-phase, and described the liquid-like L_α-phase above $T_c = 43°C$. Tardieu *et al.*[3,4] using unoriented samples confirmed their findings and found the ripple-phase $P_{\beta'}$ between 35°C and T_c. Janiak *et al.*[5] reported a temperature dependence of the tilt angle in unoriented DPL-layers. Their studies were done on systems of over 20 wt.% water, keeping the main- and pretransition at the temperatures significant for fully hydrated layers.[6] Oriented freestanding samples of 2 and 10 wt.% water content were analyzed at room temperature by Stamatoff *et al.*[7] giving a directly determined tilt angle of 12.5° for the 10% case. The ripple-phase $P_{\beta'}$ of randomly oriented DPL-multilayers was examined by Graddick *et al.*[8] and Stamatoff *et al.*[9] Several calculations of the electron-density across the Lecithin bilayers have been carried out and are discussed by Worthington and Kare.[10] Neutron diffraction was applied to oriented and unoriented DPL-samples in order to find out the chain conformation by Zaccai *et al.*[11] and the head group conformation by Büldt *et al.*[12] A recently observed sub-phase, discovered by Chen *et al.*[13] occurs near 0°C when cooling down and vanishes at 12°C after heating up.[14,15,16] DPL and other Lecithins, as well as other Phospholipids building up model membranes were subject to a large number of investigations with other methods. Some of the results in the present investigation have already been published.[17,18]

It is the aim of this paper to present more information by use of higher oriented samples and to take into account their paracrystalline nature. One then obtains a deeper insight not only into the structure of the several phases, but also into the mechanism of phase transitions. This investigation may demonstrate the utility of the theory of paracrystals for liquid crystals as well. Rinne was the first to introduce the word "paracrystal" for structures inbetween crystalline substances and isotropic melts.[19] He wrote: "Paracrystals are closely related to crystals and so justifiably closely related in nomenclature, with their one- or two-dimensionally periodic structure instead of a space lattice." It is interesting to note that Rinne also considered Lecithin as paracrystalline. Hermann, at the same time, developed the concept of "mesophases" with help of the group theory.[20] In this journal Hosemann and Müller later on demonstrated that Hermann's concept is a special case of the paracrystal theory.[21] This theory introduces nine liquid-like statistical parameters g_{ik} into a three-dimensional point lattice which

define the relative fluctuations g_{ik} of the lattice cell vectors a_i and a_k by

$$g_{ik}^2 = \overline{(a_i - \bar{a}_i, \bar{a}_k)^2}/(\bar{a}_k)^4 \quad (1)$$

In C. Hermann's theory of mesophases g_{ik} has only values 0 or >0.3. How can paracrystalline structures be found? The theory shows that the paracrystalline distortions cause a quadratic increase of the integral widths δb of the reflection with higher order h of the reflection[22]

$$\delta b = 1/\bar{d}(1/\bar{N} + (\pi g h)^2); \qquad g = (\overline{d^2}/\bar{d}^2 - 1)^{1/2} \quad (2)$$

$\bar{N}$ is the mean number of netplanes and d is the distance between molecules of adjacent netplanes in the direction of the normal to their netplanes. The same relation holds for the long period P of Lecithin bilayers. It must be added that the swelling of the DPL-multilayers was performed in the gel-phase in order to establish a well equilibrated system in this temperature range. Therefore our data are not necessarily comparable to those of DPL-samples swollen in the L_α-phase, as done by others.

II. PREPARATION AND MATERIAL

Sample preparation[17,18] was carried out with FLUKA DL-β, γ-dipalmitoyl-α-lecithin of 99.8% purity without further purification. From preliminary microscopic observations between crossed polarizers we have found the orientation to be best and the "oily streaks" to be reduced when the multilayer stack is the thinnest possible. Therefore, a mixture of DPL- and 20 wt.% of double distilled water was sandwiched in mylare films of 5μm thickness and at 60°C well compressed between glass slides, followed by the next sandwich on top of the first, etc., giving finally a "multi-sandwich" of 100 multilayer stacks, each of them 5μm thick. At room temperature the hardened 1 mm high system was cut to a 1 × 10 mm stripe whose ends were enclosed into a drop of epoxy. At this stage of preparation, the water content was diminished to approximately 10%. In order to raise the water content, the sample was stored in a water-saturated atmosphere for 50 h at 4°C. The swelling was chosen to be in the gel-state for the hydration-barrier at 20 and 30 wt.% of water[6] to be avoided and to have a well hydrated and equilibrated system in that phase. A monohydrated DPL-dummy was stored in the same way for comparison of the water content, which by gravimetric methods was found to have 26 wt.%. A more precise analysis of the water content in the sample was performed later with the help of the small angle diffraction data. Finally the multi-sandwich was sealed in a X-ray quartz capillary and mounted on a sample holder of the X-ray pinhole camera (Kiessig) for small angle scattering, which was temperature controlled. Wide and small angle scattering were recorded simultaneously on two planar filmpacks at different distances. In order to have Bragg condi-

tions for the well aligned membranes, the sample had to be oscillated by $\pm 12°$ about its long axis, being perpendicular to the X-ray beam. Ni-filtered CuKα radiation was taken from a RIGAKU RU 200 rotating anode generator driven on a 0.3 mm micro beam focus. Exposures were taken in steps of typically 3°C, starting at 0.3°C. After changing the temperature the sample was allowed to stand for at least 20 h prior to X-ray exposure.

III. RESULTS

1) Hydrocarbon lattice

Temperature dependent small and wide angle spacings and tilt angles of hydrocarbon chains are given in Figure 1. Contrary to preliminary presentation[17,18] of these data, domain I has been chosen to reach up to 14°C in accordance with new findings of the sub-phase $L_{\sigma'}$.[13-16] The splitting of

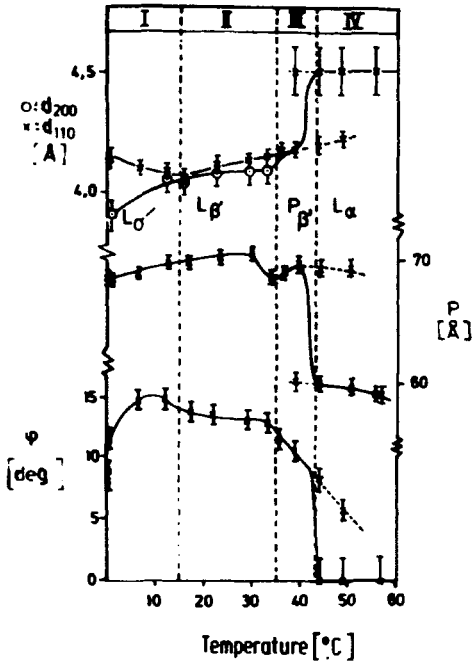

FIGURE 1 The four temperature regions of lecithin with 23 wt.% water. d_{200} and d_{110} distance in HC-lattice chains. P long period. φ angle between the normal of the membrane surfaces and the chain direction. The paraffin-like "Sub-phase" near 0°C is assigned with $L_{\sigma'}$. Dotted lines refer to the phase-separation.

the (110)- and (200) spacing has a maximum of 0.3°C, where in the sub-phase the lattice is very similar to paraffine. Here the lattice cell is orthorhombic with $a/b = 1.59$,[18] whereas paraffin as a/b = 1.49.[23] Going towards the $L_{\beta'}$-phase in domain II the split of the two spacings is about 1% only, making $a/b = 1.71$; therefore often referred to in literature as "pseudo-hexagonal."[24] Figure 2 shows the density map of CH_2-reflections at 33.8°C, well separated near the equator E, where the (200)-reflection is outside the (110)-circle. In domain III, the lattice is clearly hexagonal as shown by Graddick *et al.*,[25] but for convenience the orthorhombic nomenclature is kept. The domains I to III are often called the "gel-phase."

Above 43°C in domain IV, the L_α-phase represents the wellknown liquid-crystalline structure of molten chains with a liquid-like disorder inside the membrane. The dotted line in Figure 1 represents residual parts of the gel-phase which shall be discussed as phase separation. The distance of CH_2-chains is 8% larger in this state.

2) Membrane period

At the long spacings of the layer-period P the graph shows the most significant change at the main transition $T_c = 43$°C as well. The drop from 69 Å to 60 Å is due to chain melting, as commonly known. A residual

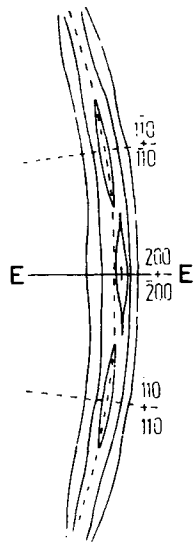

FIGURE 2 Splitting of the equatorial CH_2-reflections in domain II into three parts due to the chain tilting in b-direction. E-E is the equator.

69 Å spacing in the L_α-phase in connection with a weak 60 Å spacing below T_c gives information about a broad main transition. The pretransition at 35°C is positioned in accordance with others, but contrarily accompanied by a drop of P by 2 Å.

3) Tilt angle

The tilt angle φ shown in Figure 1, was derived from the splitting angle θ between the (200)- and the (110)-reflections (see Figure 2). Since θ is not generally φ, the direction of the tilt relative to the CH_2-lattice has to be known in order to derive φ, the tilt angle. Simple geometric considerations give the relation between the two angles. Figure 3a shows the orthorhombic cell projected on to the a-b-plane, where the c-axis is perpendicular to the paper with a length of two C-C-bonds, that is 2.5 Å, and in direction of the chain-axis. Figure 3b is the reciprocal lattice of 3a. Turning this around axis 1 causes the $(\bar{1}10)$- and (110)-reciprocal lattice points to l_y above the paperplane and the respective $(1\bar{1}0)$- and $(\bar{1}\bar{1}0)$-positions to l_y below. A rotation of the lattice about the normal of the lamellae consequently causes these lattice points to meet the Ewald-sphere of reflection twice above the equator (the plane parallel to the lamellae), twice on it and twice below it. In the case of a hexagonal lattice Levine used

$$\sin \theta = \pm \sin 60^\circ \sin \varphi^{1,2} \tag{3}$$

assuming the axis 1 (or a hexagonal equivalent one) in our Figure 3 being the tilt axis. This explains the four reflections outside the equator and the two lying on it.

In an orthorhombic lattice Eq. (3) has to be replaced by

$$\sin \theta_1 = \pm \sin \alpha \cdot \sin \varphi, \qquad \cos \alpha = \frac{d_{110}}{2d_{200}}$$
$$\sin \theta_2 = \pm 0 \tag{4}$$

If $d_{110} = d_{200}$ we have Eq. (3). Since in Figure 2 all reflections have equal intensities and widths, Eq. (4) was applied to find the tilt angle φ. The axis of tilt is the a-axis, thus the direction of the tilt is the b-direction in Figure 3a. In Figure 1, lower plot, the tilt angle rises coming from the sub-phase and reaches a maximum of 15° before reaching a plateau of 13° in the $L_{\beta'}$-phase. It is new that the sub-phase, whose CH_2-lattice is paraffin-like, has a much smaller tilt angle than in the $L_{\beta'}$-phase. In domain III φ is reduced to about 10° and becomes zero in domain IV.

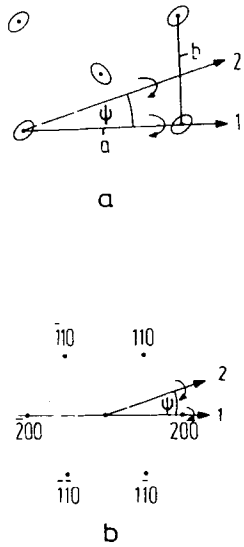

FIGURE 3 a) Orthorhombic lattice cell with edges a and b. b) Its reciprocal lattice. 1 is the observed tilt axis of the HC-chains and 2 an arbitrarily chosen tilt axis.

4) Effective water content

The long spacings P of domains I and II are about 5 Å larger than found by others.[1-5,26,27] This difference can only be due to interlamellar water. By swelling the lamellar Lecithin below T_c, the main transition temperature, we had no problems with the so-called "hydration barrier."[6] Our observations gave evidence that at room temperature very pure DPL in bidistilled water within 18 h swells up to 97 wt.% water content. The process is sensitive on ion concentration, as in 1 mmol NaCl-solution only 95.5% is the hydration barrier. In order to avoid the inhomogeneity problems of gravimetric and spectroscopic[1,2] methods, we chose to find the thickness W of the interlamellar water in domains I to III from

$$W = P - L \cos \varphi \tag{5}$$

where P is the longspacing period, L = 55,4 Å the known length of the DPL molecule[3] and φ the tilt angle of them. Within the errors of experiment W constantly is 16 Å ≙ 23 wt.% in the phases I to III.

In the L_α-phase a different approach is necessary to find the membrane thickness D, since L is not known. P is reduced by 9 Å at T_c and the

distance of the hexagonal (100) netplanes (they still exist in a liquid)[28] rises from 4.18 Å to 4.52 Å. With the known increase in volume of $\Delta V = 1{,}4\%$[29] we have for the membrane thickness

$$D = (1 + \Delta V)\frac{4.18^2}{4.52^2} L \cos\varphi = 48 \text{ Å}^{18} \tag{6}$$

D is reduced by 6 Å. In addition, the surface of the membrane is enlarged by the factor $4{,}52^2/4{,}18^2 = 1{,}17$. The assumption that the water stays between the bilayers then requests that W is reduced by this factor, by 2.3 Å. Thus the reduction of P by 6 Å + 2.3 Å ≈ 9 Å is completely explained by the fact that in our multilayer system the interlamellar water volume is constant through all phases.

5) Paracrystalline distortions of the longspacing

In the gel-phases the long period reflections become diffuser with increasing order l of reflection. The δb-l^2 plot (Figure 4) with help of Eq. (2) leads to bundles with

$$g = 0.024 \qquad \text{and} \qquad N = 45 \pm 10 \tag{7}$$

In domain IV several sharp reflections are observable and

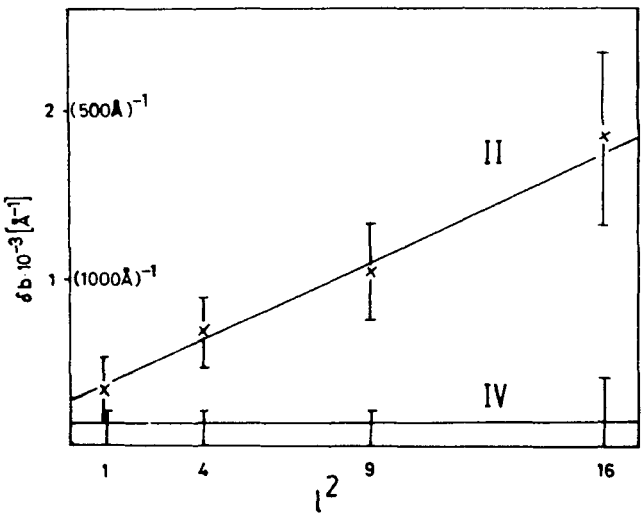

FIGURE 4 Integral widths δb against the squared order l of reflections. The long period P indicates paracrystalline distortions with $g = 2.4\%$ in domain II ($L_{\beta'}$) and unmeasurable small distortions in domain IV (L_α) with $g = 0$.

$$g < 0.01; \qquad N > 150 \tag{8}$$

Another fundamental relation exists in paracrystalline compounds, the so called α^*-law:[34]

$$\sqrt{N}g = \alpha^* = 0.15 \pm 0.03 \tag{9}$$

It proves that the size of paracrystalline lattices depends on its g-values, because the netplanes (in this case the lamellae) come more and more under shear stress. With increasing N they finally break. Here from Eq. (9) one obtains

$$\alpha^* = 0.16$$

which is in good agreement with earlier findings.

6) Phase separation

Under the given conditions of water content, the gel-phase swelling and thin multilamellar sandwiches as described, phase separation occurs between 39°C and 49°C, around the main transition. In this range the intensity of the sharp (110)-reflection of the gel-phase x diminishes, while the broad liquid scattering ⊗ becomes stronger with rising temperature as pointed out in Figure 5, where integral intensities are used. For control, the sum of both ⊡ is constant. Although this is a good proof of phase separation, the

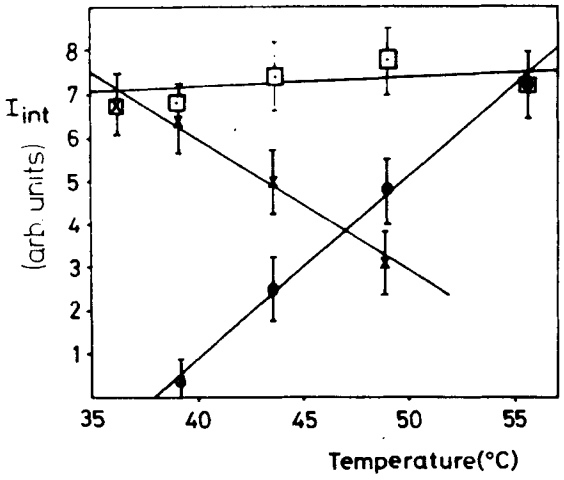

FIGURE 5 Integral intensities of CH_2-reflections of the gel-phase (x), the liquid-crystalline phase ⊗ and their (constant) sum ⊡ near the main transition temperature demonstrating a phase-separation.

quotient of the intensities of the $L_{\beta'}$-component and the L_{α}-component was taken for wide x and small $\odot$ angle reflections and found to be equal at all temperatures where the two longspacings P are observable (Figure 6). This refers to the phenomenon of a splitted period P that Stamatoff *et al.*[9] interpreted by the shape factor of ripples.

7) Significance of the tilt direction

At room temperature, between the sub- and pretransition, around 20°C the intensity of the (200) wide angle reflection diminishes markedly (Figure 7). As we have argued before, in case of a tilt in direction b, the intensity of the six reflections should be equal. Any change in this condition should be understood by a different or undefined tilt direction. Stamatoff *et al.*[7] in oriented DPL multilayers of 10% water content, observed not only a low equatorial intensity, but no peak wherefrom they assumed randomly distributed tilt directions. According to their calculation they found a tilt angle φ of 12.5° which is almost identical to our measurement. Recalculating their conversion factor between φ and the angle 2θ between their two reflections outside the equator we found it to be 0.87 which is sin 60° as we used in Eq. (4). Thus, if the angular splitting 2θ of the two outer equatorial reflections is known, then the calculated tilt angle φ is the same in both cases, whether the tilt direction is the b-direction or a disoriented one.

8) The phenomenon of ripples

Another interesting observation can be made from the width δb_1 of the lateral tails of the long period third order reflections shown in Figure 8. In

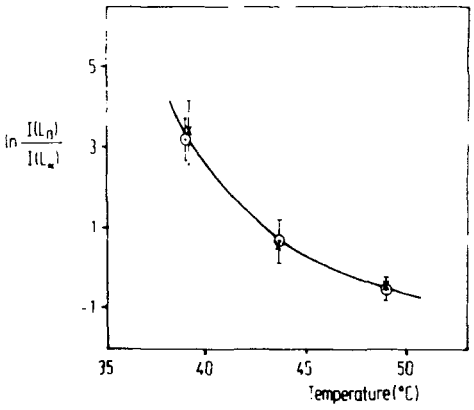

FIGURE 6 Intensity relation of the two phases near the main transition of wide- (x) and small angle ⊡ scattering in logarithmic presentation, assuring for phase separation.

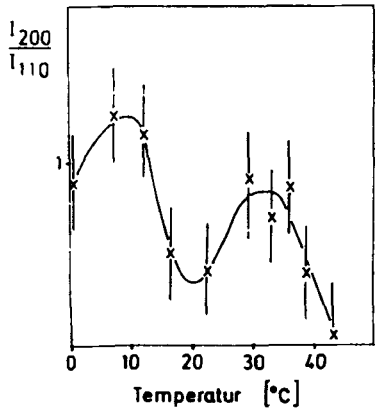

FIGURE 7 Intensity relation of the (200)- and (110)-reflection. If I(200)/I(110) = 1, then a is the tilt axis and b the tilt direction of the CH_2-chains.

range III a remarkable peak exists which will be explained below as a consequence of special ripple zones in multi-sandwich-samples of Lecithin.

According to Figure 1 φ slowly decreases with increasing temperature; now the number of $c/2$ shifts decreases with rising temperature. The stabilizing (012)-netplanes now are destroyed step by step. Molecular-dynamical phenomena may play a role. This resembles the fact that the long period P does not decrease monotonously in domain III, but has a relatively sharp peak at the end of domain III. Now one is concerned with clustering effects: The $c/2$ steps are no longer statistically distributed but cluster to build waves, the so-called ripples firstly observed by Pinto da Silva[37] in 1971.

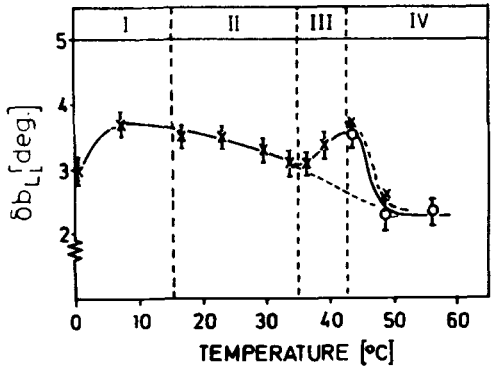

FIGURE 8 Lateral width of the third order reflection of the long period P, indicating a general decrease of disorientation of lamellae with rising temperature. The significant peak of region III is caused by the ripple structure.

IV. ANALYSIS AND DISCUSSION

1) Membrane period and hydration

We have analyzed a well oriented* DPL multilayer system which was hydrated up to a 16 Å interlamellar layer of water corresponding to 23 wt.%. By the take-up of water below the main transition temperature T_c, we find a membrane period P of 70 Å there and of 60 Å above T_c. Other workers have never reported 70 Å in the gel-phase, but usually around 65 Å.[1-5,26,27] We are sure that the large longspacing is not due to our multi-sandwich preparation, since by comparison with unoriented DPL samples swollen in the gel-phase we have found $P = 73$ Å. This, together with our observation that swelling at room temperature is not stopped before 97 wt.%, water is taken up, indicates that in the gel-phase there is no strong hydration barrier below this amount, as observed in the L_α-phase at 20% and 30% water content.[12] The X-ray measurements were started at 0.3°C near the swelling temperature of 4°C, in order to have well equilibrated conditions, and the next temperature step for the same reason was applied to the sample at least 20 h prior to X-ray diffraction. The reproducibility of data was checked by going back to 0°C, after room temperature was reached before, and then comparing the two sets of data. No difference was seen between the first and second circle. The lowering of the temperature from that of the L_α-phase to room temperature reproduces only similar spacings but not tilt angles. In general, the history of the sample seems to play a bigger part when measurements were taken at falling temperatures.[22,29] Therefore we restricted ourselves to data taken at rising temperatures. The interlamellar water volume remained constant through all phases.

2) The hydrocarbon lattice of the gel-phases

The relevant progress obtained from oriented DPL multilayers is due to the separation of the (200)- and the (110)-reflections which makes it easy to measure directly the tilt angle φ of the hydrocarbon chains with respect to the layer normal as shown in Figure 1. The little differences between d_{110} and d_{200} prove that there is an orthorhombic CH_2-lattice in the $L_{\beta'}$-phase with only 1% difference to the hexagonal case. This explains the asymmetric profiles found in unoriented samples by Janiak *et al.*[5] In the $P_{\beta'}$-phase of domain III the CH_2-lattice is clearly hexagonal, but there is still

*The degree of orientation expressed by the angle of texture was typically 3,5° FWHM (full width at half maximum).

a tilt angle of $\varphi \sim 10°$. The pretransition in accordance to Comeron *et al.*[30] and Janiak *et al.*[24] is characterized by the change from an orthorhombic to a hexagonal lattice. Rotation of the CH_2-chains about their long axis is often assumed to be the reason for the hexagonal packing.[30,14] A hindered rotation is proposed by NMR-studies of Blinć *et al.*[31] and Davis[32] and by the IR-spectroscopy of Cameron[30] even in the $L_{\beta'}$-phase. Consequently, we propose that the subtransition[13] is correlated to a stop to hindered rotation and the lattice is paraffin-like, especially confirmed by big differences of the d_{200} and the d_{110}-spacings as seen by others as well.[15,16] New about the subtransition is the strong reduction of the tilt angle φ to be 8° near 0°C (see Figure 1). As we have argued before,[18] headgroup hydrational forces might be lowered and result in a smaller tilt of chains. A reduced hydrational state is discussed by Ruocco *et al.*[16]

3) Stabilizing netplanes and tilt direction

Near the upper subtransition temperature at 12°C we find a maximum in the tilt angle φ which is 15°. Considering this to be an angle of some stabilizing meaning, we can explain it by the following mechanism: In the gel-phases of domains I to III the CH_2-chains are always tilted in the direction of the b-axis. Supposing that each chain adjacent to another one on the b-axis is shifted along the c-axis by $c/2$ (see Figure 9) then φ is given by

$$tg\varphi = \frac{c}{2b} \tag{10}$$

With $b = 4.8$ Å and $c = 2.5$ Å, we have from Eq. (10) $tg\varphi - 0.26$ and $\varphi = 15°$. The shift by $c/2$ requests a twist of the adjacent chain by 180° about its long axis, thus zig-zag fits to zig-zag. The lamellae surface then is parallel to the (012)-netplanes of the CH_2-lattice; such stabilizing net-

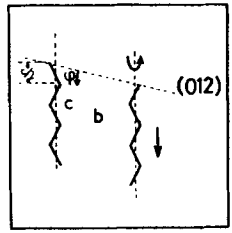

FIGURE 9 Structural explanation of a tilt angle $\varphi = 15°$. If adjacent chains are shifted by $c/2$ along their c-axis and turned around it by 180°, they can lock in and form a stabilized (012)-netplane surface.

planes were also observed in Cerebrosides.[42] Phrenosina, for instance, at 23°C partly consists of a structure I with $\varphi = 30°$ and stabilizing (201)-paraffin-netplanes. At 66°C another structure, III, appears with $\varphi = 45°$ and stabilizing (301)-netplanes. In paraffins as well, stabilizing netplanes form membrane surfaces.[43] The described mechanism reminds us of Doniach[33] who used c-steps in order to explain 30° tilt angles in his ripple model. Furthermore, it is known from neutron diffraction[11] that $3/4\ c$-shifts between the two CH_2-chains of the Lecithin molecule relate to this phase. In the $L_{\beta'}$-phase a constant tilt angle of 13° occurs which can be explained by (0, 7, 16) netplanes or, put differently, by $-c/2$-steps interrupting the (012)-netplane after 8 adjacent chains in b-direction.

4) Other tilt directions

The phenomenon demonstrated in Figure 8 where the tilt direction is less defined just above the substransition at 16°C, could be caused by the instability after the 012-netplane is no more the stabilizing surface. Only little variations of the tilt direction cause significant changes of the intensity of the equator reflection. The rise in IR-CH_2-scissoring Cameron *et al.*[30] reported near 20°C can be correlated to this, since it indicates a stronger rotation causing possibly some deviations from the b-direction.* The geometrical treatment of the problem of a tilt axis, which is not the a-axis but has an angle ψ, like the axis 2 in Figure 3 gives the relation

$$\sin\theta = f(\psi)\sin\varphi^{18} \tag{11}$$

[which is more general than Eq. (4)] where

$$f(\psi) = \pm\sin(\psi \pm \alpha); \qquad \psi \leq \frac{\pi}{2} \qquad \alpha = \begin{cases} \arccos \dfrac{d_{110}}{2d_{200}} \\ 0 \end{cases} \tag{12}$$

If $\psi = 0$ or $\pi/3$ we have Eq. (4) and there are six reflections, four outside and two on the equator, as shown before. In the general case a graph of $f(\psi)$ in Figure 10 demonstrates the different tilt directions.

If ψ is $\pi/6$ or $\pi/2$, then we have eight reflections; otherwise we have twelve. Overlaps of reflections, however, hinder the observation of twelve reflections. Thus, if like in our case, the b-direction is not exactly met, a decrease in equator intensity is to be expected. Disoriented tilt direction causes four reflections.[7]

*Our finding was presented by Helfrich at Aspen (1980).

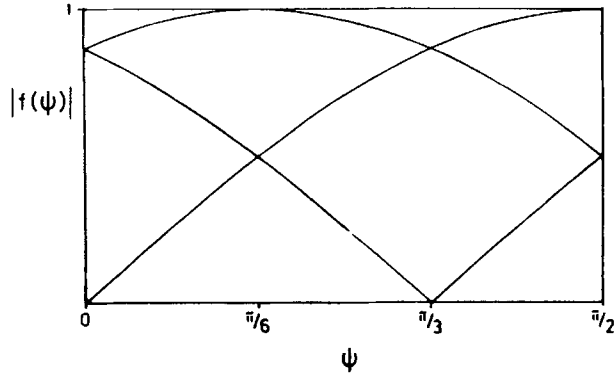

FIGURE 10 Function f (ψ) connecting the tilt angle φ of chains with θ, the angular splitting of the (110)- and (200)-reflections in Eqs. (11) and (12). If $\psi = 0$, then b is the tilt direction giving a total of six reflections. Generally 12 are possible.

5) Bilayer period statistics and Astbury's rule

As pointed out in Figure 4 the membrane period is paracrystalline distorted in the gel-phases with a disorder value $g = 2.4\%$ and $N = 45$ bilayers, bound to a bundle of thickness ~3000 Å.* The disorder does not exist in the L_α-phase; the membrane reflections are crystalline. The same feature was observed in unoriented samples, which we had hydrated over 50 wt.% water content.

In domain I–III the value g is large because, obviously, the chains are shifted statistically against each other in c-direction. The roughness of the lamellae surfaces gives rise to the larger g-values in Eq. (2). Our own observations of the (002)-reflection at $d_{002} = 1.26$ Å in oriented DPL-samples support the explanation that CH_2-chains latch onto each other. The roughness caused by the relative shift of the two chains in one lecithin molecule, which is ¾ according to Zaccai *et al.*,[11] causes part of such a g-value: ¾ $c = 1.8$ Å for every second chain giving a relative standard deviation $g = 1.8\%$. If, on the other hand, the liquid-like CH_2-chains in the L_α-phase lose some crystalline-like lateral contact to each other, then they are able to build up lamellae with a minimum surface free energy and g becomes zero, according to Eq. (2).

The schematic drawing of Figure 11 is an illustration of Astbury's rule:[35] The more disordered the molecules, the better they aggregate to super-

These data once again confirm the α-law[34] as formulated in Eq. (9), to be valid for longspacings in lamellar systems as well.

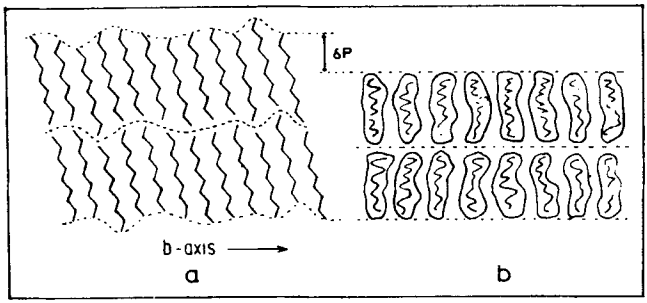

FIGURE 11 Astbury's rule demonstrated by lecithin bilayers (schematical drawing with no headgroups shown): a) $L_{\beta'}$-phase: Crystalline HC-chains, statistically latched on to each other, build up paracrystalline distorted membrane layers. b) L_{α}-phase: Paracrystalline distorted HC-chains form smooth membranes with a crystalline-like long period P.

structures and vice versa: the better the crystalline order, the worse their superstructure. Figure 11, for clarity, does not show the lecithin headgroups. Our model is a special example for Astbury's rule as it can give an answer to the question of by what mechanism this rather astonishing rule is governed in lamellar systems, *e.g.* smectic liquid crystals, polymers, and biopolymers. This example demonstrates that the paracrystalline model, which has found only "limited utility in the study of liquid crystals," leads indeed to "new insights into the structural characteristics of mesophases."[36]

6) Weak ripples of the $P_{\beta'}$-phase

Several works have been done on ripples. X-ray analysis of ripples was applied to unoriented samples first by Tardieu,[3,5] later on by Janiak[5,24] and Stamatoff.[9] Detailed electron microscopy was performed by Sackmann *et al.*[38] and Copeland *et al.*[39] Theoretical approaches were proposed by Helfrich,[40] Doniach,[33] and Larsson.[41] In the work of Janiak *et al.*,[24] which was done on dimyristoyl-lecithin, a complete indexing of the two-dimensional macrolattice was possible, contrary to Stamatoff *et al.*[9] who detected solely (h0)- and (0l)-reflections, l giving the order of the ripple period and h the order of the membrane period (our notation). In order to illustrate the diffraction of ripples, Fraunhofer-patterns of sinusoidal models are presented in Figure 12. The density of the membranes in their average plane is uniform in Figure 12a. Consequently, no equatorial reflections (h0) appear in their transform (Figure 12b). The membranes of Figure 13a have density fluctuations of half the wave length, which can be caused by changing the tilt angles of the CH_2-chains, as proposed by Helfrich.[40] Their diffraction pattern (Figure 13b) yields equatorial reflections of the half wave length (h = even number).

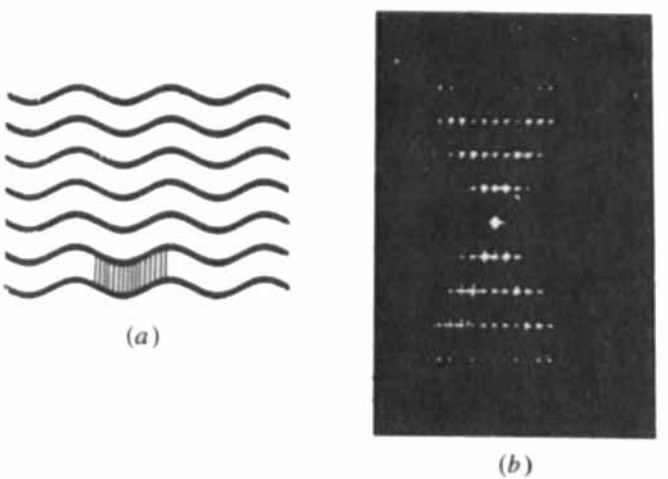

FIGURE 12 a) Idealized two-dimensional model of a ripple structure. The CH_2-chains stand parallel to the membrane normal and $\varphi = 0$. Hence there is no longitudinal density fluctuation. b) Its Fraunhofer pattern. The amplitude A of the ripples is 1/5 of the long period P. The 5th order reflection $l = \pm 5$ is zero because here the shape factor S^2 of the lamellae disappears and no equatorial reflections exist.

In our investigation we only observed a widening of the lateral tails of the $(0l)$-reflections of the bilayer stacking period appearing between 36° and 43°C in domain III. Figure 14 shows the increase in the lateral widths

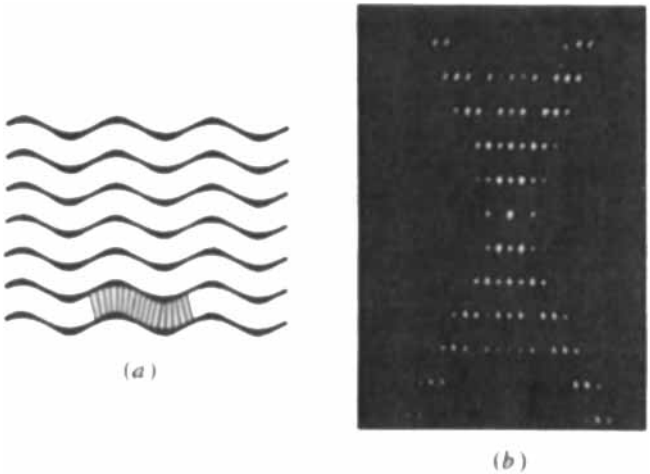

FIGURE 13 a) Two-dimensional model of ripples including density fluctuations, *e.g.* by locally tilted chains and b) its optical diffraction analoge performing equatorial reflections caused by density periods of half the ripple wave length.

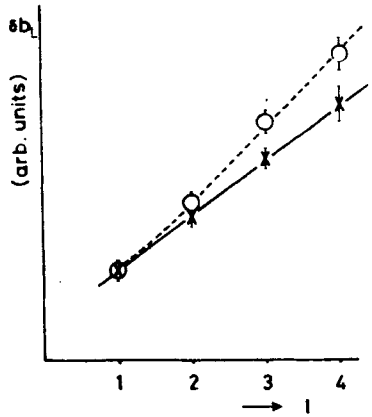

FIGURE 14 Lateral integral width δb_L of the small angle meridional reflections ($0l$). At 34°C they increase linearly with the order l of reflection (××××). At 39°C they are additionally broadened by the ripples (oooo).

δb_l of the several orders l of the stacking period at 34°C, where it increases linearly, and at 39°C, where additional broadening occurs from ripple-like structures, which probably are badly correlated and therefore give no separation between the ($0l$)- and the ($h1$)-reflections. Nevertheless, we shall analyze this type of "weak" ripples.

7) Analytical treatment of ripples

Figure 15 shows an ensemble of rod-like particles whose chains have an angle φ with the normal of the lamellae and the steps of the lamellae surface build up a "ripple" with a wavelength a. For convenience we assume that all blocks have the same thickness t. By introducing orthogonal coordinates, $P(x_2 - 0)$ is a point function in x_2-direction with

$$P(x_2 - 0) = 0 \quad \text{for} \quad |x_2| \geqq \varepsilon; \qquad \int P(x_2 - 0)\, dx_2 = 1 \tag{13}$$

ε is a quantity in the order of the equipment resolution. Thus a single ripple can be mathematically defined by a streak function (Figure 15):

$$St(x_1, x_2) = P(x_2 - A \cos 2\pi x_1/a) \tag{14}$$

Its two-dimensional Fourier transform is given by (see Appendix)

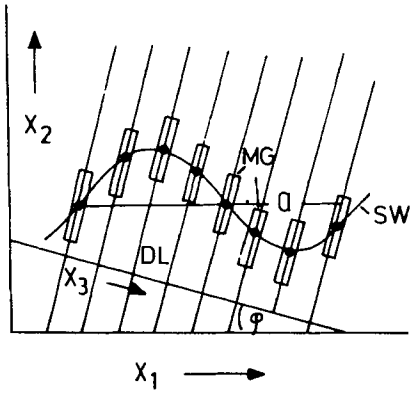

FIGURE 15 Ripple wave of molecules tilted by an angle φ in wave direction. The centres (. . . .) of the molecule groups (MG) are defined by the cross points of the sinoidal wave (SW) and the disc lattice (DL).

$$\begin{aligned}\gamma St &= \int e^{2\pi i b_2 A \cos 2\pi \cdot x_1/a} e^{2\pi i b_1 x_1}\, dx_1 \\ &= \int \sum_{n=0}^{\infty} (iq2\cos 2\pi x_1/a)^n/n! e^{2\pi i b_1 x_1}\, dx_1 \\ &= \sum_{n=0}^{\infty} \frac{(iq)^n}{n!}\left[P_{-n} + \binom{n}{1} P_{-n+2} + \ldots \binom{n}{n-1} P_{n-2} + P_n\right] \qquad (15)\end{aligned}$$

where

$$P_n = P(b_1 - n/a), \qquad q = \pi b_2 A \quad \text{and} \quad b = 2\sin\vartheta/\lambda$$

(2ϑ scattering angle, λ wavelength).

This function consists of point-like stripes parallel to the b_2-axis with

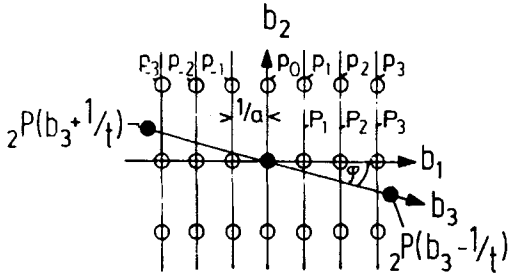

FIGURE 16 Fourier transform of the ripple structure of Figure 15. For detail see text.

distances $1/a$ (see Figure 16). For $n = 0$ only one stripe exists at $b_2 = 0$ with the weight 1. To this stripe the summand $n = 2$ adds a quadratic term

$$\frac{(iq)^2}{2!}\binom{2}{1}P(n = 0)\,.$$

The stripe at $b_1 = 1/a$ is given by

$$\left[iq + \frac{(iq)^3}{3!}\binom{3}{1} + \frac{(iq)^5}{5!}\binom{5}{2} + \ldots\right]P^1$$

So we finally obtain

$$\gamma St = \sum_{n=0}^{\infty}(iq)^n P_n \sum_{r=0}^{\infty}\frac{(iq)^{2r}}{r!(r+n)!} \tag{16}$$

The black points in Figure 15 indicate the centers of single blocks. They can be easily obtained by multiplying the function $St(x_1, x_2)$ with a lattice function:

$$z(x_3) = \sum_{m=n}^{+n} P(x_3 - mt) \tag{17}$$

where the x_3-axis has an angle φ with x and l is the distance between the molecule groups MG. The Fourier transform of $z(x_3)$ is given by

$$\gamma z(x_3) = \sum_m {}_2P(b_3 - m/t) \tag{18}$$

${}_2P$ now are two-dimensional point functions and b_3 is parallel to x_3. If one multiplies $St(x_1, x_2)$ with $\gamma z(x_3)$, then one obtains the centers of all blocks which are the black points in Figure 15. If the lamellae are smooth like in Figures 12 and 13 $z(x_3)$ is a streak function of length and orientation of a chain molecule and $\gamma(z_3)$ is a streak along the b_3-axis.

The Fourier transform of this product is, according to the Appendix, nothing else than the convolution product of $\gamma z(x_3)$ with γSt.

$$\gamma(St)\gamma z_3 \tag{19}$$

This means that function γSt of Figure 16 is superimposed by other functions $\gamma St(x - x_3/t)$ which in the Fourier space are shifted along the direction b_3 by m/t (Figure 16). Now we have to replace the point-like centers of the blocks by their shape. This can be done by folding the product of Eqs. (14) and (17) with the shape of the blocks. If $f(b)$ is the Fourier transform of their shape, then, according to the folding theorem of the Fourier transform, the intensity function is given by the product of $f^2(b)$ with Eq. (19).

The next step is to build up a bundle of such rippled lamellae. According to the theory of paracrystals, one has to multiply the total formula

by the macrolattice function $Z(b)$. Its maxima are the well-known long period reflections whose widths δb, according to Fig. 2, depend on the g-value of this superlattice. So we finally obtain, for the intensity of an oriented sample

$$I(b) \cong [f^2 \gamma St \gamma z_3 \cdot Z(b)] S^2 \tag{20}$$

S^2 is the shape factor of the bundle. It is to be folded with the bracket. Every peak of $I(b)$ has a shape S^2

$$I(b) = f^2 \sum_{n=0}^{\infty} (iq)^n \sum_{r=0}^{\infty} \frac{(iq)^{2r}}{r!(r+n)!} P_n Z(b) S_n^2 \gamma(z_3) \tag{21}$$

This expression can be easily understood if one also introduces the peaks P_n of the long period in Figure 16.

8) Discussion of ripples

Stamatoff[9] has observed in unoriented samples, in addition to a long period reflection, three very weak peaks at 165 Å and 110 Å and a stronger one at 55 Å.This can be easily explained by Figure 16 if $\varphi \neq 0$. The streak along the b_3-axis then crosses P_n-lines which all are unlike zero and explain the reflections observed by Stamatoff. On the other hand, if $\varphi = 0$, except for $P(b_3 - 0)$, the $\gamma(z_3)$-streak is multiplied with zero and no longitudinal reflections occur. This is the case in our lecithin. Moreover, the two reflections ${}_2P(b_3 - 1/t)$ and ${}_2P(b_3 + 1/t)$, cannot be observed because the single shifted groups of molecules MG (see Figure 15) touch each other, and hence, the Fourier transform $f(b)$ of their shapes (see Eq. 20) has the zero value. Figure 12a shows a model with $\varphi = 0$ and Figure 12b its Fraunhofer pattern. The weak reflections obtained by Stamatoff are produced by the two $\gamma(St)$-components whose centers are given by ${}_2P(b_3 - 1/t)$ and ${}_2P(b_3 + 1/t)$. The strong term S_0^2 of this term gives rise to the peak at ~55 Å and the weak peaks are produced by S_1^2 and S_2^2 of this shifted $\gamma(St)$-function. The ripple wavelength is then given by 165 Å, according to Stamatoff, and the thickness t of the shifted blocks is about a third part of the ripple wavelength. This means that, contrary to the multi-sandwich, where such interferences could not be observed, here the blocks are tilted against the normal of the lamellae. If, in our case, φ really becomes zero in domain III, then the ripple waves must go along the a-axis of the paraffin-lattice. If not, the ripple has at least a component in the b-direction. Therefore, it cannot be decided what really happens. On the other hand, Tardieu[3] and Janiak[5] only observed satellites of the long period

(p_1 and p_{-1} in Figure 16) which indicate $\varphi = 0$ and a relatively uniform wavelength. Herefrom they found a wave length

$$a = 141 \text{ Å}.$$

Eq. (21) explains the $I(h, l)$ reflections which all have the same Cauchy-shape S_n^2 if, as in the L_α-phase, the g-value of the superlattice is zero (Figure 4). They are smeared out by the texture effect explained above. One obtains their smeared shape directly by analyzing the $(0l)$-reflections at 34°C with a microdensitometer. At 39°C the line profile changes to the Cauchy-shape with an exponent 1.5 which can be explained by two additional S_n^2-reflections, according to Eq. (21). This separation is performed in Figure 17 with the help of a DuPont 310 curve resolver for the 4th order of the meridional reflection. The analysis is absolutely satisfying if one introduces solely the reflections $(0l)$, $(1l)$ and $\bar{1}l)$. This is the first hint that one only needs the terms $r = 0$ of Eq. (21).

$$I(p, l) = \sum_p (\pi A l/P)^{2p} S_p^2/p! \tag{22}$$

because A/P is so small that the terms $|r| \geqq 0$ can be neglected. Another proof for

$$A/P \ll 1 \tag{23}$$

is given by Figure 18: The weights of the second maxima S_1^2 divided through S_0^2 give a straight line if plotted against l^2. From $l = 4$ one obtains quantitatively

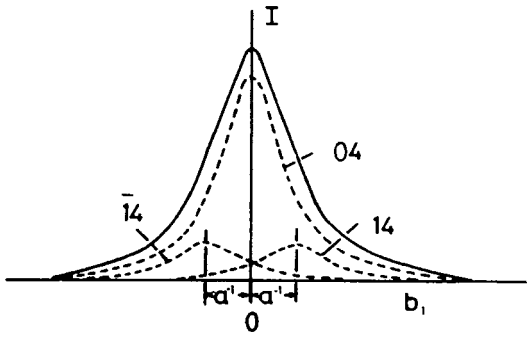

FIGURE 17 Construction of the rods S_0^2, S_1^2 and S_{-1}^2 corresponding to the (04)- (14)- and the (14)-reflections in the ripple domain at 39°C using the profile S_0^2 of the $(0l)$-reflection at 34°C.

$$\frac{I(1.4)}{I(0.4)} = (\pi A 4/P)^8 = 0.18\,, \qquad \text{hence } A/P = 0.06 \pm 0.01 \tag{24}$$

and

$$A = (4.5 \pm 0.5)\ \text{Å}$$

For $l=2$, 3, and 4 the positions of the S_l^2 peaks are nearly identical and indicate that the mean wave length of the ripples is given by

$$\bar{a}=(310\pm30)\ \text{Å} \tag{25}$$

From the discussion of Copeland and McConnel[39] it is known that the wavelength of ripples can be the multiple of another observed wavelength and differs with preparation techniques. Therefore, the wavelength and amplitude observed are not generally representative. We wanted to demonstrate the method of analysis.

The value $\bar{a}=310\pm30$ Å is the mean value of an ensemble of strongly varying wavelengths. This large variance may be due to the special preparation of the multi-sandwich which, due to the activities of the mylar foils, hinders the growth of ripples with a well-defined wavelength.

Coming back to the concept of paracrystalline structures, one can explain the diagram of Figure 15 in a more statistical way also: The distance distribution $H(\mathbf{x})$ of the vectors $\mathbf{x}$ expanded between the centers of adjacent bimolecules gives a statistical fluctuation $\Delta^2(\mathbf{x}, p)$ in the direction of the longer period P

$$\Delta^2(x,p) = \int H(\mathbf{x})\,(\mathbf{x} - \bar{\mathbf{x}}\,, s_p)^2\, dx^3 \tag{26}$$

where s_p is a unit vector in the direction of P. The integral width δg_{exp} of the long period reflections in the lateral direction then is given by

$$\delta b_{\text{exp}} = 1/\bar{\mathbf{x}}(1/\bar{N} + (\pi g_{\text{exp}} l)^2 \tag{27}$$

where

$$g_{\text{exp}} = \Delta(\mathbf{x}, p)/P$$

and $\bar{N}$ is the mean number of bimolecules within one lamella (see Eq. 2). From Figure 18, one obtains

$$\frac{\delta b(l=4) - \delta b(l=1)}{\delta b(l=1)} \sim 4 \tag{28}$$

hence

$$(\pi g_{\text{exp}} 4)^2 = 4\,; \qquad g_{\text{exp}} = 0.16 \tag{29}$$

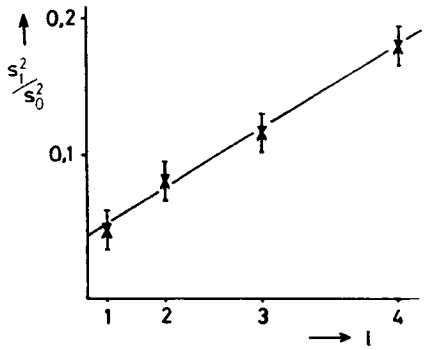

FIGURE 18 Quotient S_1^2/S_0^2 which is $I(1l)/I(0l)$ in the ripple domain. The slope indicates that $A/P \sim 0.06$ (see text).

The bimolecules, hence, fluctuate statistically at the end of section III in s_p-direction by $\Delta(x, p) = 10$ Å. There is no doubt that in reality there may exist correlations between these fluctuations which create a field of large varying wavelengths whose average value is given by ~310 Å. Nevertheless, both explanations — Figure 12, confirming a widely varying wave, length with a mean wavelength $\bar{a} = 310$ Å and the paracrystalline concept of uncorrelated step dislocations — lead to the result that in the multisandwich sample in section III special, more or less correlated, or uncorrelated relations exist between the positions of adjacent bimolecules.

Acknowledgment

We are much indebted to the Deutsche Forschungsgemeinschaft and to the Freie Universität Berlin who supported our work. Moreover, we gratefully acknowledge valuable discussions with W. Helfrich.

The Fourier transform of the one-dimensional function $P(x_2 - a)$ is defined by

$$\gamma P(x_2 - a) = \int P(x_2 - a) e^{-2\pi i b_2 x_2} dx_2$$

From Eq. (13) it follows that

$$\gamma P(x_2 - a) = e^{-2\pi i a b_2}$$

The Fourier transform of the one-dimensional function $2 \cos 2\pi x_1/a$ therefore is given by

$$\gamma 2\cos(2\pi x_1/a) = \gamma(e^{+2\pi i x_1/a} + e^{-2\pi i x_1/a}) = P(b_1 - 1/a) + P(b_1 + 1/a)$$

The folding theorem of the Fourier transformation is defined by

$$\gamma(gh) = GH = \int G(c)H(b-c)\,dc; \qquad G = \gamma g; \qquad H = \gamma(h)$$

Putting $g = h = 2\cos 2\pi x_1/a$ one obtains

$$[P(b_1 + 1/a) + P(b_1 - 1/a)][P(b_1 + 1/a) + P(b_1 - 1/a)] = P(b_1 + 2/a) + 2P(b_1 - 0) + P(b_1 - 2/a)$$

Using this binomial folding process one finally obtains the last line of Eq. (15).

References

1. Y. K. Levine, *Progr. Biophys. Mol. Bio.*, **24**, 3 (1972).
2. Y. K. Levine, *Progr. Surf. Sci.*, **3**, 279 (1973).
3. A. Tardieu, Thesis, Université Paris Sud, Centre d'Orsay (1972).
4. A. Tardieu, V. Luzzati, and F. C. Reman, *J. Mol. Biol.*, **75**, 711 (1973).
5. M. J. Janiak, D. M. Small, and G. G. Shipley, *Biochem.*, **15**, 4575 (1976).
6. L. Powers, P. S. Pershan, *Biophys. J.*, **20**, 137 (1977).
7. J. B. Stamatoff, W. P. Graddick, L. Powers, and D. E. Moncton, *Biophys. J.*, **25**, 253 (1979).
8. W. F. Graddick, J. B. Stamatoff, P. Eisenberger, and N. Spielberg, *Biochem. Biophys. Res. Comm.*, **88**, 907 (1979).
9. J. B. Stamatoff, Abstract, 25th Annual Meeting, Denver 1981, *Biophys. J.*, **33**, 2 (1981).
10. C. R. Worthington and R. S. Kare, *Biophys. J.*, **23**, 407 (1978).
11. G. Zaccai, G. Büldt, A. Seeling, and J. Seelig, *J. Mol. Biol.*, **134**, 693 (1979).
12. G. Büldt, H. U. Gally, J. Seelig, and G. Zaccai, *J. Mol. Biol.*, **134**, 673 (1979).
13. S. C. Chen, J. M. Sturtevant, and B. J. Gaffney, *Proc. Natl. Acad. Sci. USA*, **77**, 5060 (1980).
14. L. Trahms, W. Klabe, and E. Boroske, *Biophys. J.* (in press).
15. H. H. Füldner, *Biochem.*, **20**, 5707 (1981).
16. M. J. Ruocco and G. G. Shipley, *Biochim. Biophys. Acta*, **684**, 59 (1982).
17. M. Hentschel, R. Hosemann, and W. Helfrich, *Z. Naturforsch.*, **35a**, 643 (1980).
18. M. Hentschel, Thesis, Freie Universität Berlin (1981).
19. F. Rinne, *Trans. Act. Farad. Soc.*, **292**, 1016 (1933).
20. C. Hermann, *Z. Krist.*, **79**, 186 and 337 (1931).
21. R. Hosemann and B. Müller, *Mol. Cryst. Liq. Cryst.*, **10**, 273 (1976).
22. R. Hosemann and S. N. Bagchi, *Direct Analysis of Diffraction by Matter*, North-Holland Publ. Comp., Amsterdam (1962).
23. C. W. Bunn, *Trans. Farad. Soc.*, **35**, 482 (1939).
24. M. J. Janiak, D. M. Small, and G. G. Shipley, *J. Biol. Chem.*, **254**, 6068 (1979).
25. W. F. Graddick, J. B. Stamatoff, P. Eisenberger, and N. Spielberg, *Biochem. Biophys. Res. Comm.*, **88**, 907 (1979).
26. J. Torbet and M. H. F. Wilkins, *J. Theor. Biol.*, **69**, 447 (1976).
27. K. Furuya and T. Mitsui, *J. Phys. Soc. Jap.*, **46**, (1979).

28. B. Steffen and R. Hosemann, *Ber. Bunsen-Ges. Phys. Chem.*, **80**, 710 (1978).
29. H. Träuble and D. H. Haynes, *Chem. Phys. Lipids*, **7**, 324 (1971).
30. D. G. Cameron, H. L. Casal, E. F. Gudgin, and H. H. Mantsch, *Biochim. Biophys. Acta*, **596**, 463 (1980) and *Biochem.*, **19**, 3665 (1980).
31. R. Blinć, M. I. Burger, V. Rutar, B. Zeks, R. Kind, H. Arend, and G. Chapuis, *Phys. Rev. Lett.*, **43**, 1679 (1979).
32. J. H. Davis, *Biophys. J.*, **27** (1979).
33. S. Doniach, *J. Chem. Phys.*, **70**, 4587 (1979).
34. R. Hosemann and F. J. Baltá-Calleja, *Ber. Bunsen-Ges. Phys. Chem.*, **84**, 91 (1980).
35. W. T. Astbury, *Nature*, **137**, 803 (1936).
36. L. V. Azároff, *Mol. Cryst. Liq. Cryst.*, **60**, 73 (1980).
37. P. Pinto da Silva, *J. Micros.*, **12**, 185 (1971).
38. E. Sackmann, D. Rüppel, and C. Gebhardt, *Liquid Crystals of One- and Two-dimensional Order*, Springer-Verlag, Berlin (1980).
39. B. R. Copeland and H. M. McConnel, *Biochim. Biophys. Acta*, **599**, 95 (1980).
40. W. Helfrich, *Z. Naturforsch.*, **29c**, 692 (1974).
41. K. Larsson, *Chem. Phys. Lipids*, **20**, 225 (1977).
42. S. Fernandez-Bermudez, J. Loboda-Čačković, H. Čačković, and R. Hosemann, *Z. Naturforsch.*, **33c**, 362 (1977).
43. O. Phaovibul, H. Čačković, J. Loboda-Čačković, and R. Hosemann, *J. Polymer Sci.*, **11**, 2377 (1973).